Hetero-Trihalides

Bonding Analysis in Homo- and Hetero-Trihalide Species: A Charge Displacement Study

Gianluca Ciancaleoni*[a] Massimiliano Arca,[b] Giovanni F. Caramori,[a] Gernot Frenking,[c] Felipe S. S. Schneider,[a] and Vito Lippolis[b]

Abstract: The bonding in homo- (X_3^-) and hetero-trihalides (XYX^-), with X = F, Cl, Br, and I; Y = I, has been analyzed through the charge displacement (CD) method, coupled with energy decomposition analysis (EDA). We focus our attention on how the different bond components vary with the distance between the terminal and the central halogen atoms. The results clearly show that all the homo-halide systems X_3^- feature the same trend of the charge transfer (CT) versus the asymmetry of the three-body system, defined as the ratio between the two bond lengths d_{X1-X2} and d_{X2-X3}, whereas in the case of the hetero-

trihalides $BrIBr^-$ and $ClICl^-$, the CT values are similar, but systematically lower with respect to the homo-trihalide case. Comparison with solid-state geometries also allows us to estimate the influence of the crystal lattice (the packing and the interactions with the surrounding fragments) on the geometry. Following the results reported here, the CD method is confirmed to be a useful alternative computational tool to analyze the nature and the origin of weak intermolecular interactions such as halogen and hydrogen bonding.

Introduction

The nature of the chemical bond in linear three-body systems, such as trihalides, has been the subject of renewed interest recently.[1,2] In fact, these systems featuring a central halogen atom are currently classified as cases in which halogen bonding (XB, the interaction between a polarized halogen atom and a Lewis base)[3] occurs, and the understanding of the chemical bond in trihalides can, therefore, help to disembroil the ongoing debate on how to define the XB, and to understand its origin, similarities, and differences from other weak intermolecular interactions.[4,5] In particular, the paper by Hoffmann and co-workers published in 1997[6] analyzed, on the basis of density functional calculations, the various contributions to the stabilization of trihalides by comparing the Rundle–Pimentel model[7] for electron-rich three-centered four-electron (3c, 4e) systems with that describing the interhalogenic bond as a donor/acceptor or charge-transfer interaction between a halide and a dihalogen molecule. Later, Mealli and co-workers extended the work to polyiodide systems.[8] Although it is not easy to assign the contribution of each energy term to the bonding in these hypervalent anions, both models account for

a total bond order of 1 in these systems, and, although the former fits better for symmetric systems, the latter describes better strongly asymmetric arrangements.

These conclusions are nicely supported by the structural features retrieved from the Cambridge Structural Database (CSD) for linear three-body systems involving either trihalogens, X–X–X (X = Br, I), or halogen(s) and chalcogen(s), E–X–Y, X–E–Y, and E–X–E (E = S, Se; X = Y = Cl, Br, I; X = I, Y = Cl, Br). The relative elongations (δ) of the two bonds in the examined three-body systems with respect to the sum of the relevant covalent radii show a continuous variation from balanced situations to very unbalanced ones without indications of the critical distances at which the bonds switch from a substantially covalent to a predominantly electrostatic nature. Furthermore, all data can be fitted by a common nonlinear least-squares equation derived from the bond-valence model (BV).[9]

To give a rationale to this structural variability, it is interesting to know exactly how the bond changes with the interatomic distance. For example, it is known that the total energy of trihalide ions changes slowly with the distance between the central and one of the terminal elements, thus justifying the existence of the great variety of structures aforementioned.[10]

For this reason, in our work we focused our attention on how the different bond components vary with the internuclear distance. To do this, we chose to quantify the charge transfer (CT), recognized as an important component to halogen bonding,[11–13] through the charge displacement (CD) method.[14] This already proved to be useful for the characterization of coordinative[15] and non-covalent bonds,[16] including halogen and chalcogen bonding.[17] Such a method, which is exclusively density-based, is demonstrated to be stable with the basis set size, the functional, and the level of theory to account for the

[a] Departamento de Química, Universidade Federal de Santa Catarina, 88040-900 Florianópolis, SC, Brazil
E-mail: g.ciancaleoni@ufsc.br
http://www.qmc.ufsc.br

[b] Dipartimento di Scienze Chimiche e Geologiche, Università degli Studi di Cagliari,
S.S. 554 Bivio per Sestu, 09042 Monserrato (CA), Italy

[c] Fachbereich Chemie, Philipps-Universität Marburg,
Hans-Meerwein-Strasse, 35032 Marburg, Germany

📄 Supporting information and ORCID(s) from the author(s) for this article are
ⓘ available on the WWW under http://dx.doi.org/10.1002/ejic.201600471.

ChemPubSoc
Europe

EurJIC
European Journal
of Inorganic Chemistry

Full Paper

relativistic effects (scalar or full four-component Hamiltonian).[15b,15d] It is also important to underline that, by using the CD method, the charge displacement can be computed in each point, therefore allowing us to quantitatively analyze the polarization within each fragment.[15c,18]

For a more thorough analysis, we coupled the CT with the energy decomposition analysis, in combination with the natural orbital for chemical valence method (EDA-NOCV[19]).

Computational Details

All the optimizations and the charge displacement calculations were carried out by using density functional theory employing the mPW1PW functional[20] as implemented in Gaussian 09, the Ahlrichs polarized quadruple-ζ def2-QZVP basis set,[21] and the multiconfiguration Dirac–Hartree–Fock (MCDHF) adjusted small-core pseudo-potential for iodine.[22] All the totally relaxed structures, namely **X(s)**, are confirmed as energy minima, showing only positive vibrational frequencies. When necessary, the polarity of the medium has been modeled through the polarizable continuum model (PCM) procedure[23] to check its effect on the geometries (Figure S15, Supporting Information).

The charge displacement analysis relies on [Equation (1)]:

$$\Delta q(z') = \int_{-\infty}^{\infty} dx \int_{-\infty}^{\infty} dy \int_{-\infty}^{z'} dz\, \Delta\rho(x,y,z) \tag{1}$$

where $\Delta\rho(x,y,z)$ is the difference between the electron densities of a complex (X_3^-) and the sum of that of its non-interacting fragments (X^- and X_2), frozen at the same geometry they assume in the complex. The term $\Delta q(z')$ defines at each point z' along a chosen axis the amount of electron charge that moves through a plane perpendicular to the given axis through z. Accordingly, a positive slope describes regions of charge accumulation, whilst a negative slope denotes charge depletion. To characterize the interaction with only one value of Δq, it is useful to fix a plausible boundary separating the fragments in the adducts. Unless otherwise specified, we chose the isodensity value representing the point on the z axis at which equal-valued isodensity surfaces of the isolated fragments are tangent. At this point, the value of Δq is represented by CT. At the midpoint of the X_2 bond, the value of Δq is represented by P_{2-3}. The CD method proved to be very stable with the choice of the functional or the basis set.[15b,15d]

The EDA-NOCV[19] calculations were performed by using the model BP86-D3/TZ2P+ as the level of theory,[24] as implemented in the ADF2013 package.[25] EDA-NOCV combines the extended transition state method, ETS,[26] with the natural orbitals for chemical valence scheme NOCV.[27] In such a scheme, the instantaneous interaction energy, ΔE^{int}, is decomposed according to Equation (2) into the following components: ΔE^{elstat}, which corresponds to the quasi-classical electrostatic interaction between the interacting fragments, by keeping their frozen charge distributions. The term ΔE^{Pauli} provides the Pauli repulsion between occupied orbitals of the interacting fragments.

The term ΔE^{orb} gives both the charge transfer between interacting fragments, by evaluating the interaction between occupied orbitals from one fragment with the unoccupied orbitals of the other fragment, and also the polarization of the same fragment. As the BP86-D3 functional is employed, the dispersion correction, ΔE^{disp}, is included into the total interaction energy [Equation (2)]. The EDA-NOCV scheme is derived from Nalewajski–Mrozek[28] valence theory, and therefore links the concepts of bond order, bond orbitals, and charge reorganization with the deformation density.

$$\Delta E^{int} = \Delta E^{elstat} + \Delta E^{Pauli} + \Delta E^{orb} + \Delta E^{disp} \tag{2}$$

The differential density, $\Delta\rho(r)$, is decomposed by the NOCV pairs (Ψ_{-i}, Ψ_i) into the contributions $\Delta\rho_i(r)$ [Equation (3)], where v_i and N stand for the NOCV eigenvalues and the number of basis functions. The eigenvalues, v_i, provide the charge estimation for a given deformation density, $\Delta\rho_i(r)$, that means, $\Delta q_i = |v_i|$. The deformation density plots give information about the symmetry and the direction of the flow of charge. In the EDA-NOCV scheme, the orbital component can be specified in terms of v_i eigenvalues [Equation (4)], where F_{ii}^{TS} are the diagonal transition-state Kohn–Sham matrix elements defined over NOCV eigenvalues. In this case, ΔE_i^{orb} provides the energetic estimation of $\Delta\rho_i(r)$ related to a particular electron flow channel. Further details about EDA-NOCV can be found in the literature.[26,27]

$$\Delta\rho(r) = \sum_{i=1}^{N/2} v_i \left[-\psi_{-i}^2(r) + \psi_i^2(r) \right] = \sum_{i=1}^{N/2} \Delta\rho_i(r) \tag{3}$$

$$\Delta E^{orb} = \sum_i \Delta E_i^{orb} = \sum_{i=1}^{N/2} v_i \left[-F_{-i,-i}^{TS} + F_{i,i}^{TS} \right] \tag{4}$$
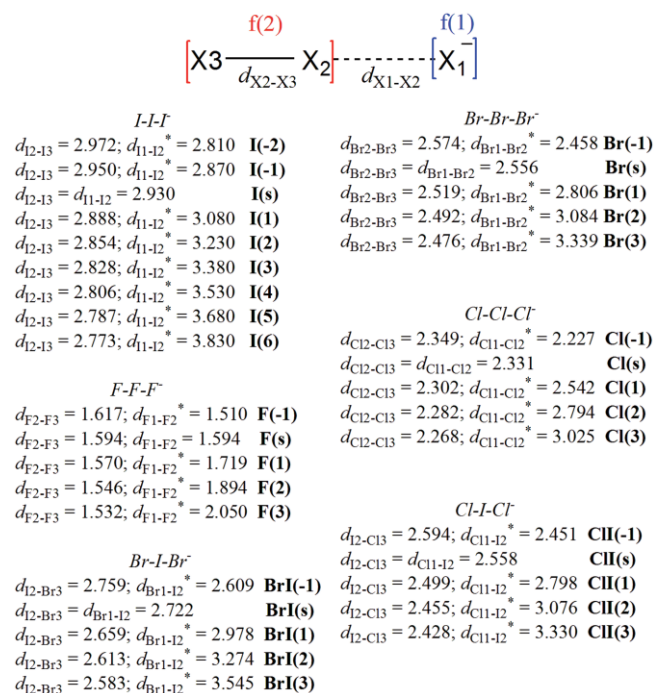
To check the dependence of the EDA-NOCV results on the functional, the analysis has been carried out for the system ClICl$^-$ also with the local meta-GGA TPSS functional[29] corrected by applying the D3 London dispersion correction with Becke–Johnson damping[24] (TPSS-D3). The numeric differences between the two functionals are generally lower than 1.0 kcal mol^{-1} (Table S2, Supporting Information).

Results and Discussions

The I_3^- macro-anion has been optimized in the gas phase by using the mPW1PW functional, which already proved to perform well for halide systems,[30] the MCDHF-adjusted small-core pseudo-potential and the def2-QZVP basis set (see Computational Details). In the equilibrium structure, **I(s)**, the geometry is symmetrical with $d_{I-I} = 2.930$ Å (Scheme 1).

The bond dissociation energies for **I(s)** to $I_2 + I^-$ or to $I_2^- + I$ are 44.7 and 60.7 kcal mol^{-1}, respectively (see the Supporting Information). The former is more favorable than the latter; therefore, the fragmentation scheme for all the X_3^- (or XYX$^-$) triatomic systems considered here will be $X_2 + X^-$ (or XY + X$^-$).

Many unsymmetrical geometries of I_3^- have been partially optimized, each one with a different constrained value of d_{I1-I2} (Scheme 1). It can be seen that d_{I2-I3} decreases as d_{I1-I2} in-

★ChemPubSoc
Europe

EurJIC
European Journal
of Inorganic Chemistry

Full Paper

$$\left[X3 \underset{d_{X2-X3}}{\overset{f(2)}{\rule{3cm}{0.4pt}}} X2\right] \text{------} \overset{f(1)}{\left[X_1^-\right]}$$

$$d_{X1-X2}$$

I-I-I⁻

$d_{I2-I3} = 2.972; d_{I1-I2}{}^* = 2.810$ **I(-2)**
$d_{I2-I3} = 2.950; d_{I1-I2}{}^* = 2.870$ **I(-1)**
$d_{I2-I3} = d_{I1-I2} = 2.930$ **I(s)**
$d_{I2-I3} = 2.888; d_{I1-I2}{}^* = 3.080$ **I(1)**
$d_{I2-I3} = 2.854; d_{I1-I2}{}^* = 3.230$ **I(2)**
$d_{I2-I3} = 2.828; d_{I1-I2}{}^* = 3.380$ **I(3)**
$d_{I2-I3} = 2.806; d_{I1-I2}{}^* = 3.530$ **I(4)**
$d_{I2-I3} = 2.787; d_{I1-I2}{}^* = 3.680$ **I(5)**
$d_{I2-I3} = 2.773; d_{I1-I2}{}^* = 3.830$ **I(6)**

F-F-F⁻

$d_{F2-F3} = 1.617; d_{F1-F2}{}^* = 1.510$ **F(-1)**
$d_{F2-F3} = 1.594; d_{F1-F2} = 1.594$ **F(s)**
$d_{F2-F3} = 1.570; d_{F1-F2}{}^* = 1.719$ **F(1)**
$d_{F2-F3} = 1.546; d_{F1-F2}{}^* = 1.894$ **F(2)**
$d_{F2-F3} = 1.532; d_{F1-F2}{}^* = 2.050$ **F(3)**

Br-I-Br⁻

$d_{I2-Br3} = 2.759; d_{Br1-I2}{}^* = 2.609$ **BrI(-1)**
$d_{I2-Br3} = d_{Br1-I2} = 2.722$ **BrI(s)**
$d_{I2-Br3} = 2.659; d_{Br1-I2}{}^* = 2.978$ **BrI(1)**
$d_{I2-Br3} = 2.613; d_{Br1-I2}{}^* = 3.274$ **BrI(2)**
$d_{I2-Br3} = 2.583; d_{Br1-I2}{}^* = 3.545$ **BrI(3)**

Br-Br-Br⁻

$d_{Br2-Br3} = 2.574; d_{Br1-Br2}{}^* = 2.458$ **Br(-1)**
$d_{Br2-Br3} = d_{Br1-Br2} = 2.556$ **Br(s)**
$d_{Br2-Br3} = 2.519; d_{Br1-Br2}{}^* = 2.806$ **Br(1)**
$d_{Br2-Br3} = 2.492; d_{Br1-Br2}{}^* = 3.084$ **Br(2)**
$d_{Br2-Br3} = 2.476; d_{Br1-Br2}{}^* = 3.339$ **Br(3)**

Cl-Cl-Cl⁻

$d_{Cl2-Cl3} = 2.349; d_{Cl1-Cl2}{}^* = 2.227$ **Cl(-1)**
$d_{Cl2-Cl3} = d_{Cl1-Cl2} = 2.331$ **Cl(s)**
$d_{Cl2-Cl3} = 2.302; d_{Cl1-Cl2}{}^* = 2.542$ **Cl(1)**
$d_{Cl2-Cl3} = 2.282; d_{Cl1-Cl2}{}^* = 2.794$ **Cl(2)**
$d_{Cl2-Cl3} = 2.268; d_{Cl1-Cl2}{}^* = 3.025$ **Cl(3)**

Cl-I-Cl⁻

$d_{I2-Cl3} = 2.594; d_{Cl1-I2}{}^* = 2.451$ **ClI(-1)**
$d_{I2-Cl3} = d_{Cl1-I2} = 2.558$ **ClI(s)**
$d_{I2-Cl3} = 2.499; d_{Cl1-I2}{}^* = 2.798$ **ClI(1)**
$d_{I2-Cl3} = 2.455; d_{Cl1-I2}{}^* = 3.076$ **ClI(2)**
$d_{I2-Cl3} = 2.428; d_{Cl1-I2}{}^* = 3.330$ **ClI(3)**

Scheme 1. Nomenclature and schematic representation of homo- and hetero-trihalide geometries, including fragmentation scheme used in CD and EDA studies. Interatomic distances (d) are in Å. Asterisked distances are constrained. The distances have been chosen so as to have the same normalized distances (δ) in all the systems.

creases (Figure 1). Notably, when d_{I1-I2} tends to infinity, d_{I2-I3} tends to 2.716 Å, which is only slightly longer than the distance calculated for the isolated neutral iodine molecule (2.650 Å) and is the same value experimentally determined for iodine in the solid state.[31,32] The positive (negative) index in the name of the systems [as **I(1)** or **I(−1)**] indicates a system in which the iodide is farther (closer) to the central atom of iodine than in **I(s)**. The curve qualitatively recalls the curve shown by Bürgi in his seminal work.[33] As already found in the literature and re-
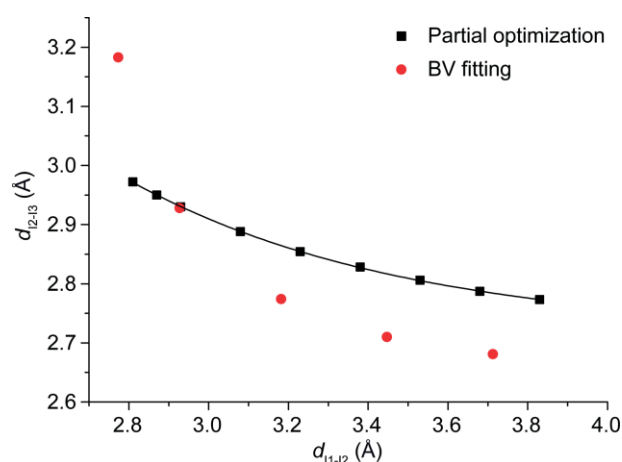

Figure 1. Black squares represent the dependence of d_{I2-I3} on (constrained) d_{I1-I2} in the I_3^- adduct. The black solid line is the best exponential fit [$d_{I2-I3} = 15.0e^{(-1.45d_{I1-I2})} + 2.715$, $r^2 = 0.9999$]. Red circles show the geometries derived from the best fit of the structural data retrieved from the Cambridge Crystal Database (CCD) following the bond-valence model.[9]

called in the Introduction, the energy of the system (Table 1) does not vary dramatically when the distance between the central and terminal iodine is modified.[10]

Table 1. Values of α, CT, and P_{2-3} (in e) and relative energies (in kcal mol⁻¹) for the partially optimized geometries of I_3^-.

	α (d_{I1-I2}/d_{I2-I3})	CT	P_{2-3}	E
I(−2)	0.945	0.416	0.487	0.82
I(−1)	0.973	0.404	0.462	0.19
I(s)[a]	1.00	0.391	0.442	0.00
I(1)	1.07	0.363	0.394	0.89
I(2)	1.14	0.337	0.354	2.93
I(3)	1.20	0.314	0.320	5.53
I(4)	1.26	0.292	0.290	8.28
I(5)	1.32	0.274	0.266	10.99
I(6)	1.38	0.256	0.245	13.52

[a] Not constrained.

Similar partial optimizations have been carried out on other homo- and hetero-trihalides, as Cl_3^-, Br_3^-, $ClICl^-$, and $BrIBr^-$ (Scheme 1). In all cases, the fully optimized geometries are symmetric [$d_{X1-X2} = 2.331, 2.556, 2.558,$ and 2.722 Å in **Cl(s)**, **Br(s)**, **ClI(s)**, and **BrI(s)**, respectively]. The other geometries have been chosen with the aim to have the same normalized distance δ_{X1-X2} (X = halogen atom),[10] see Equation (5), shown in the **I(−2)**, **I(2)**, **I(4)**, and **I(6)** systems:

$$\delta_{X1-X2} = \frac{d_{X1-X2} - (r_{X1} + r_{X2})}{(r_{X1} + r_{X2})} \tag{5}$$

where r_{X1} and r_{X2} are the covalent radii of the atomic species involved.[10]

As recalled in the Introduction, in the solid state, relative variations in the bond lengths of the trihalide geometries can be nicely fitted with an empirical equation derived from the BV model, independently of the nature of the halogen atoms involved and according to the relationship described in Equation (6):

$$\delta_{X1-X2} = -k \ln\left[1 - e^{-\frac{\delta_{X2-X3}}{k}}\right] \tag{6}$$

with $k = 0.15$.[10] But such geometries are different from those obtained by DFT optimizations (Figure 1), which is an indication that, probably, the geometries of trihalides in the solid state are strongly influenced by other factors. Apart from crystal packing and interactions with other molecular fragments, which strongly depend on the specific crystal structure and are difficult to model in a general way, the anionic nature of I_3^- can be influenced by the "polarity" of the crystal structure. Indeed, imposing a polarizable continuum model (PCM) to take into account such polarity, the partially optimized geometries becomes more similar to those obtained by using Equation (6) (see Figure S15, Supporting Information).

Charge Displacement

The $X_2\text{···}X^-$ interaction has been analyzed with charge displacement (CD) analysis.

ChemPubSoc
Europe

EurJIC
European Journal
of Inorganic Chemistry

Full Paper

The map of the difference of electron density ($\Delta\varrho$) between the adduct (I_3^-) and the sum of the electron densities of the two fragments (I_2 and I^-), frozen in the positions they assume in the adduct, allows us to qualitatively analyze how the electron density of the system changes upon adduct formation (Figure 2). The iodide ion (I1, on the right in Figure 2) shows electronic depletion, whereas the charge accumulates between the two fragments. The latter can be considered as a combination of polarization and effective charge transfer. On the other hand, the iodine molecule shows a complex pattern of alternating charge accumulation and depletion regions, indicating a strong polarization of the molecule. In particular, the combined effect of the charge decrease between I2 and I3 (the atom at the center and on the left, respectively, in Figure 2) and the charge increase on both the atoms weakens the I2–I3 bond, which is actually longer than the equilibrium bond length in the isolated I_2 (2.652 Å). Interestingly, $\Delta\varrho$ shows an almost perfect inversion center in I2 as a result of the molecular symmetry. The small asymmetry is due to the fact that I1 and I3 are not equivalent, being part of different fragments.
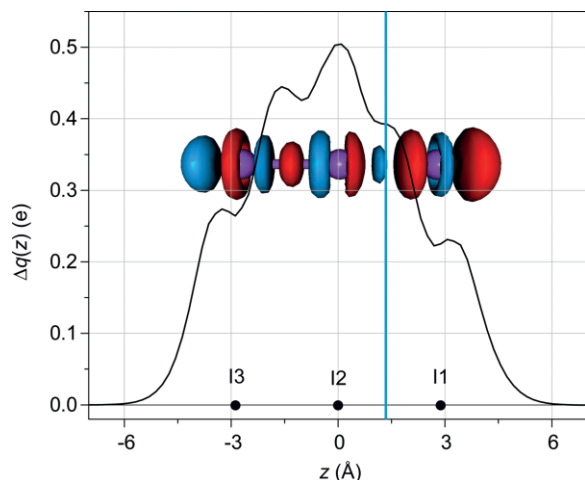
Figure 2. Charge displacement function for **I(s)**. The black dots represent the z coordinate of the atoms. The light blue vertical line identifies the boundary between the two fragments. Overprint: contour map of the change of electronic density upon formation of the complex I_3^- (equilibrium geometry, $d_{I1–I2} = 2.93$ Å) from I_2 and I^-. The direction of the charge flow is red → blue. Density value at the isosurfaces: ±0.0025 au.

By integrating $\Delta\varrho$ along the axis passing through the three atoms (z), according to Equation (1), the charge displacement function (CDF) is obtained, allowing the quantification of Δq upon adduct formation. A positive (negative) value of Δq indicates that the charge flows from right to left (left to right), providing quantitative information about the $I_2\cdots I^-$ interaction (Figure 2). In particular, the CDF for the formation of the I_3^- adduct is positive throughout the whole molecule, indicating that the electron charge flows from the iodide ion (placed on the right in Figure 2) to the iodine molecule. The value of Δq at the inter-fragments boundary (CT, see Computational Details for the choice of the boundary), is 0.391 e.

Figure 2 confirms, as already stated in the literature,[5] that the equilibrium geometry of the I_3^- anion is mainly held by a charge-transfer interaction, which, considering the short dis-

tance between I1 and I2, is not surprising, and the bond can be considered "covalent".

Analyzing the $I_2\cdots I^-$ interaction in **I(6)** ($d_{I1–I2}$ is constrained at 4.13 Å), it can be seen that $\Delta\varrho$ is qualitatively similar to that obtained for **I(s)**: the electronic density decreases on I1 and increases on I3, with a polarization of I1. All the contributions are weaker than in **I(s)**, but a certain degree of symmetry is still present. Plotting the isodensity surfaces at a lower value of density, the charge accumulation between I1 and I2 is still visible (Figure S1), together with the charge depletion between I2 and I3.

By integrating $\Delta\varrho$ for all the geometries from **I(–2)** to **I(6)**, a series of CDF curves can be obtained (Figure 3). The shape of the function does not change much as $d_{I1–I2}$ increases, except for the fact that the atom coordinates are slightly different, but the intensity of the CDF markedly decreases as $d_{I1–I2}$ increases.
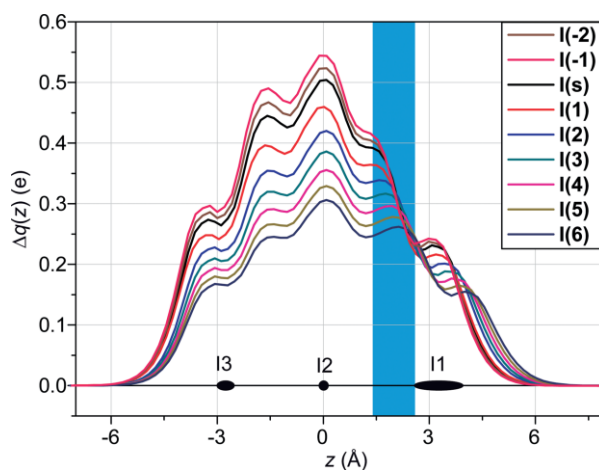

Figure 3. Charge displacement functions for I_3^- at different (constrained) values of $d_{I1–I2}$. The black dots (or bands) represent the z coordinate (or range of coordinates) of the atoms in the different geometries. The vertical band identifies the range of boundaries between the two fragments in the different geometries.

Extracting all the CT values from the corresponding CDFs, the effect of $d_{I1–I2}$ on the charge transfer can be evaluated. The CT lowers from 0.416 to 0.256 e (Table 1) as $d_{I1–I2}$ increases, and its trend can be fitted with an exponential function (Figure S2, Supporting Information).

It is interesting to underline that, if in the case of **I(s)** the CT is undoubtedly important, for **I(6)** it would be reasonable to think that the bonding is not "covalent" any more, but predominantly electrostatic and dominated by polarization. As the charge displacement method takes into account both the effects,[18] it gives a unifying vision of the bonding and is able to coherently describe all the situations.

It is also interesting to analyze the trend of CT with the asymmetry of the molecule, α. The latter can be defined as the ratio between $d_{X1–X2}$ and $d_{X2–X3}$, with $\alpha = 1$ for symmetric trihalides.

CT shows an exponential decay with respect to α, which is coherent with the fact that when I1 is very far form I2 (high values of α), the charge transfer is supposed to decrease to the limit value of zero. Coherently, the fitting equation predicts a value of only 0.04 electrons at the asymptote. Anyway, between

ChemPubSoc
Europe

EurJIC
European Journal
of Inorganic Chemistry

Full Paper

$\alpha = 0.9$ and 1.4 the function is quite flat and can also be fitted with a linear function (Figure 4). The goodness of fit of the r^2 parameter (0.9939) and the analysis of the residuals (which are less than 0.005 electrons, see Figure S3, Supporting Information) show that the use of a linear fit instead of an exponential one gives only a small error in this region.
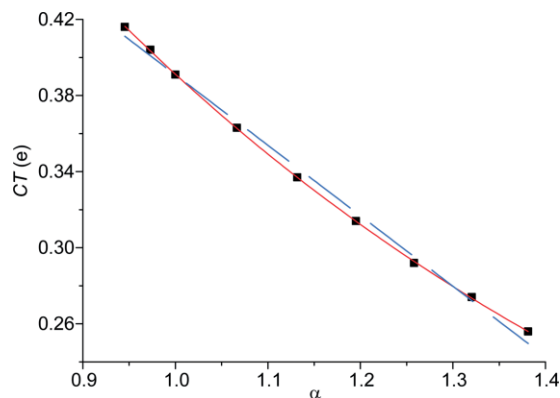

Figure 4. Dependence of charge transfer (CT) on α (d_{I1-I2}/d_{I2-I3}). The red solid line is the best exponential fit [CT = 0.04 + 1.25e$^{(-1.26\alpha)}$, r^2 = 0.9999]. The blue dashed line is the best linear fit (CT = 0.76–0.37α, r^2 = 0.9939).

Notably, Rosokha and co-workers, even if with different systems, also underlined a linear correlation between the charge transfer and the lengthening of the C–Br (or Br–Br) bond.[34]

The CD method provides not only information on the interaction between the two fragments, but also on the polarization of a fragment upon adduct formation.[15c,18] In the case of I_3^-, we can set a relationship between the CT value and the consequent polarization of the I2–I3 fragment, which can be estimated from the value of $\Delta q(z')$ at the mid-point of the I2–I3 bond (P_{2-3}). The latter is an estimation of the electronic deformation produced by the approach of an iodide to an isolated I_2. It is important to underline that such a deformation is not a consequence of the d_{I2-I3} increase, as the neutral I2–I3 fragment considered here already has the geometry assumed in the adduct. By plotting P_{2-3} versus CT, an exponential relationship can be noted, even if the trend can be satisfactorily fitted with a first degree linear equation (Figure S4, Supporting Information). Interestingly, at low values of d_{I1-I2}, P_{2-3} is even higher than CT, underlining that the electronic deformation is really strong, resulting also from the high polarizability of the iodine molecule.

The same analysis for F_3^-, Br_3^-, and Cl_3^- leads to qualitatively similar results: the corresponding contour maps of $\Delta\varrho$ are qualitatively similar to that calculated for iodine, underlining that the nature of the interaction is similar for all the homo-trihalide systems. From a quantitative point of view, the CT values computed for the symmetric geometries are almost identical for all the systems, being 0.391 for both $I_2\cdots I^-$ and $Br_2\cdots Br^-$, 0.387 for $F_2\cdots F^-$, and 0.386 for $Cl_2\cdots Cl^-$. As before, the trend of CT as a function of α has been studied, and also in this case CT decreases as α increases (Figures S5–S12, Supporting Information), but in all the cases a linear fit is still a good approximation.

Interestingly, both the slope and the intercept of all the fitting equations are very similar. As a confirmation, all the data can be plotted together (Figure 5), and they significantly over-

lap, with some scattering at high values of α. Indeed, a single fitting equation, CT = 0.73–0.34α (r^2 = 0.9694), satisfactorily describes all the data. In other words, the charge transfer needed to induce a certain asymmetry in the X_3^- conformation is the same for all three homo-trihalides. Also, the trend of P_{2-3} versus α is the same for all three systems.
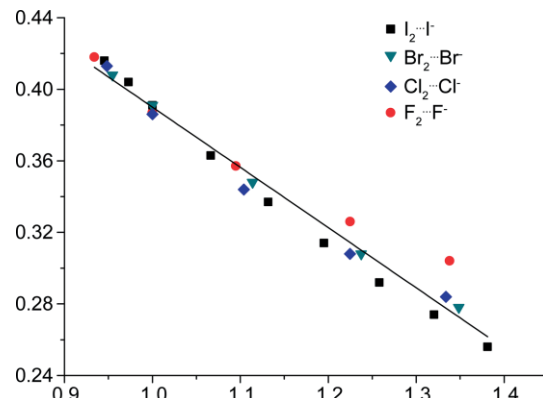

Figure 5. Dependence of charge transfer (CT) on α (d_{X1-X2}/d_{X2-X3}) for homo-trihalide systems. The red line is the best linear fit (CT = 0.73–0.34α, r^2 = 0.9694).

On passing from homo- to hetero-trihalide species, among the different possibilities we chose ClICl$^-$ and BrIBr$^-$, for which a larger database of structural data exists.[35] Optimizing their structures without any constraints, symmetric conformations are obtained (d_{Cl-I} = 2.56 Å, d_{Br-I} = 2.72 Å). Also in this case, the shape of the corresponding CDF is similar to that calculated for the homo-trihalide systems (Figures S9–10, Supporting Information), but the value of CT is now slightly different, being 0.336 and 0.363 e for ClI$\cdots$Cl$^-$ and BrI$\cdots$Br$^-$, respectively. The fact that the central atom is less electronegative than the ones at the terminal positions likely lowers the value of CT.

Analyzing the decay of CT as α increases, also in these cases the linear fitting is a good approximation. Moreover, the slopes of the best fitting equations are remarkably similar (0.34 and 0.35 for ClI$\cdots$Cl$^-$ and BrI$\cdots$Br$^-$, respectively), and strikingly similar to the slope of the fitting equation for the homo-trihalides systems (0.34, see Figure 6). On the other hand, the intercept of
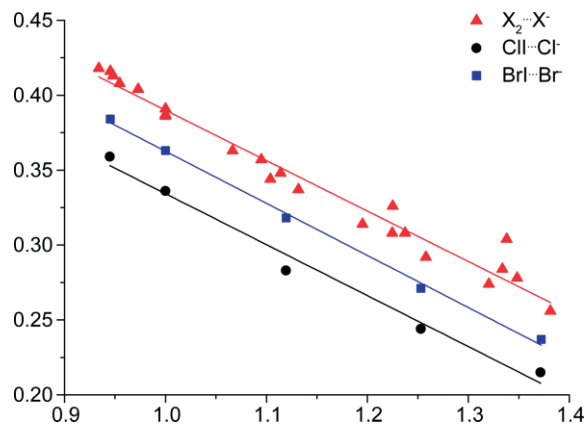

Figure 6. Dependence of charge transfer (CT) on α (d_{X1-X2}/d_{X2-X3}) for homo- and hetero-trihalide systems. The three lines are the best linear fits: for ClI$\cdots$Cl$^-$ CT = 0.67–0.34α (r^2 = 0.9799), for BrI$\cdots$Br$^-$ CT = 0.71–0.35α (r^2 = 0.9962), for homo-trihalide systems, see Figure 5.

ChemPubSoc
Europe

EurJIC
European Journal
of Inorganic Chemistry

Full Paper

the fitting line is finely tuned by the nature of the chosen halogens, even if all of them are within a range of 0.05 electrons.

In other words, to modify the asymmetry α of a trihalogen system by a certain amount, the charge transfer must change by the same amount in all cases.

EDA-NOCV

To shed more light into the similarities and differences between homo- and hetero-trihalides species, EDA-NOCV analysis was employed for all the systems depicted in Scheme 1.

The results are presented in Table 2 and reveal that the magnitude and the composition of the total interaction are dependent on the distance between X1 and X2. For all the systems, the interaction energy, ΔE^{int}, decreases as d_{X1-X2} increases, as expected. Notably, ΔE^{int} is generally larger in absolute value for lighter halogens [–51.5, –47.2, and –44.6 kcal mol^{-1} for **Cl(s)**, **Br(s)**, and **I(s)**, respectively] and for the hetero-trihalogen systems [–54.4 and –49.6 kcal mol^{-1} for **ClI(s)** and **BrI(s)**, respectively]. The only exceptions are **ClI(3)** and **BrI(3)**, in which the interactions are slightly less stabilizing than in the corresponding **Cl(3)** and **Br(3)** conformations (Table 2, for the complete table including results for F$_3^-$, see Table S2, Supporting Information).

An analysis of the energy components reveals that the increase of $|\Delta E^{int}|$ for lighter species is due to a marked stabilization in ΔE_{tot}^{orb}, which changes from –65.0 to –85.5 kcal mol^{-1} for **I(s)** and **Cl(s)**, respectively, only partially compensated by an increase in ΔE^{Pauli} and ΔE^{elstat}.

On the other hand, the difference between the homo- and hetero-trihalides is due to the electrostatic component, ΔE^{elstat}, which increases significantly on going from Cl$_2$•••Cl$^-$ (–75.0 to –11.6 kcal mol^{-1}) to ClI•••Cl$^-$,(–98.0 to –17.4 kcal mol^{-1}) and from Br$_2$•••Br$^-$ (–79.8 to –11.8 kcal mol^{-1}) to BrI•••Br$^-$ (–89.1 to –14.1 kcal mol^{-1}). This is entirely in line with the presence of a pre-formed dipole in the hetero-dihalogen molecule, with the more positive atom facing the approaching anion, as already underlined in the literature.[6,8] The enhanced ΔE^{elstat} is partially counterbalanced by a marked decrease in the orbital contribution, ΔE_{tot}^{orb}. In fact, ΔE_{tot}^{orb} goes from –85.5 and –75.3 kcal mol^{-1} for **Cl(s)** and **Br(s)**, respectively, to –70.2 and –67.1 kcal mol^{-1} for **ClI(s)** and **BrI(s)**, respectively.

All these components show an exponential relationship with the previously calculated CT (Figure S13, Supporting Information). It is interesting to note that the absolute value of all the components decays with α (Figure 7), but with different rates (–5.64, –4.95, and –3.60 for ΔE^{Pauli}, ΔE^{elstat}, and ΔE_{tot}^{orb}, respectively). This causes a variation in the composition of the relative

Table 2. EDA-NOCV results (kcal mol^{-1}) and calculated atomic patial charges q for the interactions between the halide ions f(1) and the neutral dihalogen molecules f(2) (see Scheme 1) at the BP86/TZ2P+ level.

| | Cl$_2$•••Cl$^-$ | | | | | ClI•••Cl$^-$ | | | | |
	Cl(–1)	Cl(s)	Cl(1)	Cl(2)	Cl(3)	ClI(–1)	ClI(s)	ClI(1)	ClI(2)	ClI(3)
ΔE^{int}	–51.5	–51.5	–48.2	–42.3	–36.9	–54.2	–54.4	–50.5	–43.3	–36.7
ΔE^{Pauli}	128.5	92.8	47.9	21.7	10.6	129.8	94.0	45.2	19.2	8.9
ΔE^{elstat}	–75.0	–57.3	–33.8	–18.8	–11.6	–98.0	–76.2	–44.8	–26.2	–17.4
ΔE_{tot}^{orb}	–103.5	–85.5	–60.9	–44.0	–34.6	–84.0	–70.2	–49.0	–34.6	–26.5
ΔE_1^{orb}	–91.1	–77.0	–56.5	–41.5	–32.9	–69.9	–59.9	–43.4	–31.2	–24.1
ΔE^{disp}	–1.5	–1.4	–1.4	–1.3	–1.2	–2.0	–2.0	–1.9	–1.8	–1.7
q_1[a]	–0.562	–0.581	–0.613	–0.639	–0.656	–0.622	–0.640	–0.676	–0.707	–0.728
q_2	–0.438	–0.419	–0.387	–0.361	–0.344	–0.378	–0.360	–0.324	–0.293	–0.272

| | Br$_2$•••Br$^-$ | | | | | BrI•••Br$^-$ | | | | |
	Br(–1)	Br(s)	Br(1)	Br(2)	Br(3)	BrI(–1)	BrI(s)	BrI(1)	BrI(2)	BrI(3)
ΔE^{int}	–46.5	–47.2	–44.4	–38.5	–33.0	–49.5	–49.6	–45.6	–38.7	–32.4
ΔE^{Pauli}	124.0	93.1	44.6	19.7	9.4	122.4	88.6	42.3	18.0	8.3
ΔE^{elstat}	–79.8	–62.9	–35.1	–19.2	–11.8	–89.1	–68.7	–39.3	–22.1	–14.1
ΔE_{tot}^{orb}	–88.6	–75.3	–52.0	–37.2	–29.0	–80.4	–67.1	–46.4	–32.5	–24.7
ΔE_1^{orb}	–78.0	–67.7	–48.3	–35.1	–27.5	–68.7	–58.7	–42.0	–29.9	–22.8
ΔE^{disp}	–2.1	–2.0	–1.9	–1.8	–1.6	–2.4	–2.4	–2.3	–2.1	–1.9
q_1[a]	–0.581	–0.596	–0.630	–0.657	–0.675	–0.608	–0.627	–0.664	–0.695	–0.717
q_2	–0.419	–0.404	–0.370	–0.343	–0.325	–0.392	–0.373	–0.336	–0.305	–0.283

| | I$_2$•••I$^-$ | | | | | | | | |
	I(–2)	I(–1)	I(s)	I(1)	I(2)	I(3)	I(4)	I(5)	I(6)
ΔE^{int}	–44.6	–44.8	–44.6	–42.9	–40.2	–37.2	–34.0	–30.9	–28.1
ΔE^{Pauli}	115.6	98.3	83.6	55.6	37.0	24.6	16.4	11.0	7.4
ΔE^{elstat}	–79.2	–69.0	–60.1	–43.0	–31.1	–22.9	–17.1	–13.0	–10.1
ΔE_{tot}^{orb}	–78.0	–71.1	–65.0	–52.6	–43.2	–36.2	–30.7	–26.4	–23.0
ΔE_1^{orb}	–67.5	–62.2	–57.5	–47.5	–39.6	–33.4	–28.5	–24.5	–21.5
ΔE^{disp}	–3.1	–3.0	–3.0	–2.9	–2.8	–2.7	–2.6	–2.5	–2.3
q_1[a]	–0.578	–0.588	–0.598	–0.621	–0.641	–0.658	–0.673	–0.687	–0.697
q_2	–0.422	–0.412	–0.402	–0.379	–0.359	–0.342	–0.327	–0.313	–0.303

[a] Hirshfeld charge analysis: q_1 is the charge of fragments Cl$^-$, Br$^-$, and I$^-$, whereas q_2 represents the charge of fragments Br$_2$, Cl$_2$, I$_2$, BrI and ClI.

ChemPubSoc
Europe

EurJIC
European Journal
of Inorganic Chemistry

Full Paper

contribution of stabilizing components of ΔE^{int}, ΔE^{elstat}, ΔE^{orb}_{tot}, and ΔE^{disp}. For instance, on going from **I(–2)** to **I(6)** (Table 1), the relative electrostatic contribution varies from 49.4 % to 28.5 %, whereas the orbital and dispersion contributions vary from 48.7 % to 65.0 % and from 1.9 % to 6.5 %, respectively.
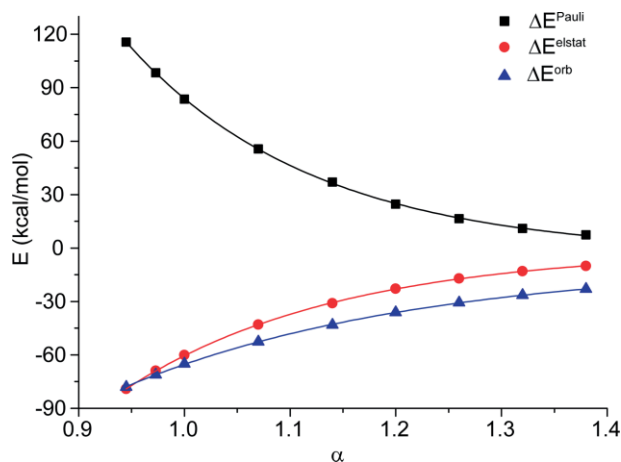

Figure 7. Trend of EDA-NOCV parameters with α for for I$^-$/I$_2$ structures.

In all systems, there is only one relevant density deformation channel, $\Delta\varrho_1(r)$ (Figure 8), which is qualitatively similar to the overall $\Delta\varrho$ (Figure 1). It arises from the ion→dihalogen donation and density polarization of the dihalogen molecule (red surfaces denote density outflow and blue surfaces denote density inflow). The donation comes preferentially from X1, as illustrated by the density depletion around the anion and the density buildup between the interacting species.

The orbital stabilization that arises from the dominant density deformation channel, ΔE^{orb}_1, involves donation from the occupied p$_z$ orbital of the anion towards the unoccupied σ* orbital of the dihalogen molecule.[6,8] The amount of charge transferred, Δq_1, goes from 0.949 to 0.665 electrons for **Cl(–1)** and **CII(3)**, respectively (Figure 8 and Figure S14, Supporting Information). These values are larger than those calculated with the CD analysis, but the same trend holds. In fact, both q_2 and the orbital stabilization, ΔE^{orb}_1, are dependent on the distance between the ion and dihalogen, and also on the nature of the ion. Generally, systems containing homo-trihalogen species present larger charge transfer and orbital stabilization than the hetero-trihalogen systems. The less significant density deformations with orbital stabilizations, ΔE^{orb}_2, ΔE^{orb}_3, and ΔE^{orb}_{res}, comprise only small density polarizations.

The analysis of the Hirshfeld charges is quite consistent with the result shown in Figure 6, with all the homo-trihalide systems showing a charge on f(2) of ca. 0.4 e [slightly higher for

Cl(s), 0.419 e], and the hetero-trihalide ones showing smaller values. More importantly, the trends evidenced by the two methods (CD and Hirshfeld) linearly correlate each other (Figure 9), as already noted previously.[17c] On the other hand, the natural population analysis (NPA[36]) systemically gives larger values for the transferred charge than CT or the Hirshfeld values. In this case, the trend of q_2(NPA) versus CT can be fitted with a line or, more accurately, with an exponential function (Figure 9).
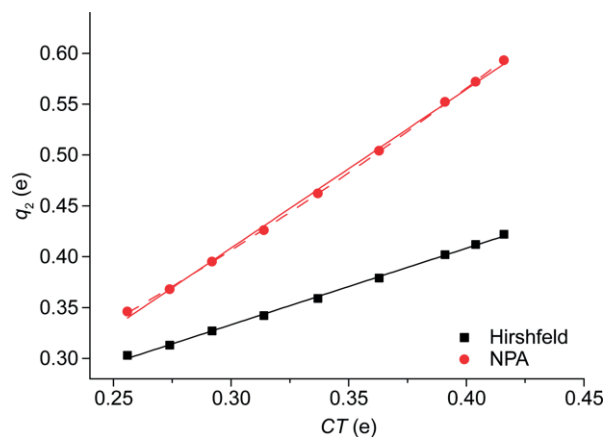

Figure 9. Comparison between the values of charge transfer (CT) according to different methods for I$^-$/I$_2$ structures. Solid (dashed) lines refer to linear (exponential) fitting. The fitting equations are: q_2(Hirshfeld) = 0.75CT + 0.107 (r^2 = 0.9984); q_2(NPA) = 1.56CT – 0.050 (r^2 = 0.9980); q_2(NPA) = –0.4 + 0.5e$^{1.8CT}$ (r^2 = 0.9998).

Considering the fully relaxed [**X(s)**] structures of different homo-trihalides, it is interesting to note that the different energy contributions have a different weight: for example, ΔE^{orb}_{tot} ranges from –85.5 (59.3 %) to –75.3 (53.7 %) and –65.0 (50.7 %) kcal mol^{-1} for chlorine, bromine, and iodine, respectively. But all of them show very similar Hirshfeld charges.

Bonding Analysis for BV Geometries

As mentioned previously, the solid-state geometries of the trihalide systems can be fitted according to the BV model and are not reproduced by DFT geometries (Figure 1). For this reason, we applied the CD method to the geometries derived from the best fitting of the structural data retrieved from the CCD according to Equation (6). The results are summarized in Table 3 (for the complete data for bromine and chlorine, see Table S4, Supporting Information). Not surprisingly, the CT value corresponding to **I$_{BV}$(s)** is very similar to that computed for **I(s)** (0.386 and 0.391 e, respectively) since, as we saw before, the
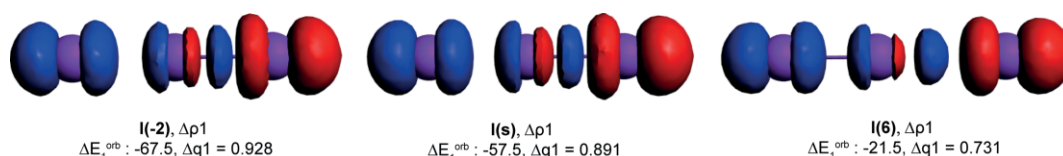

I(-2), Δρ1
ΔE^{orb}_1 : -67.5, Δq1 = 0.928

I(s), Δρ1
ΔE^{orb}_1 : -57.5, Δq1 = 0.891

I(6), Δρ1
ΔE^{orb}_1 : -21.5, Δq1 = 0.731

Figure 8. Most significant density deformation channel contributions to I$_3^-$ at selected bond lengths. The direction of the charge flow is red→blue. Anionic fragments are placed on the right (contour value 0.002) and energies are in kcal mol^{-1}.

ChemPubSoc
Europe

EurJIC
European Journal
of Inorganic Chemistry

Full Paper

two geometries are very similar. For the same reason, all the symmetric systems behave as described previously, showing practically identical values of CT [0.383 and 0.388 for **Br$_{BV}$(s)** and **Cl$_{BV}$(s)**, respectively].

Table 3. Values of normalized distances (δ_{I1-I2}, δ_{I2-I3}) and charge transfer (CT, in e) for the BV geometries of homo-trihalides.

	δ_{I1-I2}	δ_{I2-I3}	CT
I$_{BV}$(−1)	0.046	0.200	0.465
I$_{BV}$(s)	0.104	0.104	0.386
I$_{BV}$(1)	0.200	0.046	0.312
I$_{BV}$(2)	0.300	0.022	0.264
I$_{BV}$(3)	0.400	0.011	0.229
Br$_{BV}$(s)	0.104	0.104	0.383
Cl$_{BV}$(s)	0.104	0.104	0.388

Similarly to before, the trends of CT versus α nicely overlap for the triiodide, tribromide, and trichloride systems. Also in this case, the data can be fitted both with a linear or an exponential function (Figure 10), even if the linear fit in this case is worse. The corresponding equations are very different from the equations derived for the partially optimized geometries (Figures 4 and 5).
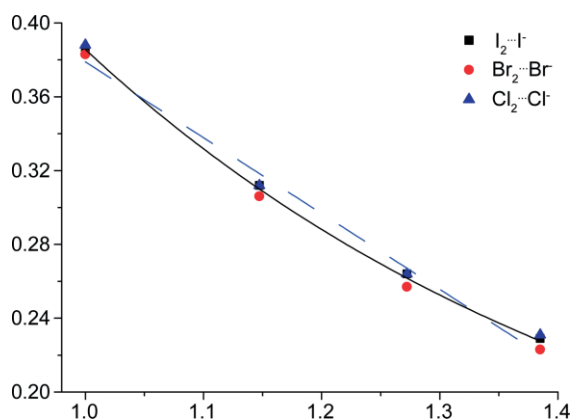
Figure 10. Dependence of charge transfer (CT) on α (d_{X1-X2}/d_{X2-X3}) for homo-trihalide systems (BV-fitted geometries). The black line is the best exponential fit [CT = 0.06 + 1.9e$^{(-1.79\alpha)}$, r^2 = 0.9996], the blue dashed line is the best linear fit (CT = 0.86−0.46α, r^2 = 0.9804).

For example, the exponent of the fitting exponential function is now −1.79, whereas previously it was −1.26. This means that the difference between the CT calculated for BV-fitted geometries, which describes well the solid-state structures of the trihalide systems, and that obtained for the DFT partially optimized geometries can be calculated at each point [Equation (7)].

$$\Delta CT = 0.02 + 1.9e^{(-1.79\,\alpha)} - 1.25e^{(-1.26\,\alpha)} \qquad (7)$$

Interestingly, such a difference is negative for $\alpha > 1$ (i.e., the CT is smaller for BV geometries than for DFT ones).[37] Therefore, the same asymmetry can be obtained in the solid state with a lower amount of charge transfer X$^-$ → X$_2$ with respect to the gas phase. This difference is likely due to the effect of the crystal lattice (mainly the packing and the other interactions of the trihalide species with the surrounding fragments) on the geom-

etry, which compensate for such a difference and provide the necessary driving force for the geometry distortion.

Conclusions

In this work, we investigated the interaction between the central (X2) and the terminal (X1) halogen atom of X$_3^-$ species, with the aim to shed some light on the large variety of geometries featured by such species in the solid state.[10] To do this, we fragmented the adduct in a halide ion (X1$^-$) and a neutral dihalogen molecule (X2–X3), which are the products of the dissociation.

We started characterizing the paradigmatic macro-anion I$_3^-$. In the fully relaxed geometry, the terminal anion I1 transfers 0.391 electrons to I2–I3, with a consequently induced polarization of the latter by 0.442 e. When constraining the I1–I2 distance, the trend of charge transfer and polarization have been shown to be exponential with the asymmetry of the structure, α, but approximately linear in the range considered here. The transition from substantially covalent (symmetric geometry) to predominantly electrostatic bonding (asymmetric geometries) was revealed to be smooth and without any discontinuity. Remarkably, the charge displacement method is able to describe both the situations, thereby giving a unifying vision of the bonding.

The analysis of the homo-trihalides F$_3^-$, Br$_3^-$, and Cl$_3^-$ showed that the trend of CT with α is very similar in all cases, independent of the nature of X. In the case of hetero-trihalides, the trends showed a systematic difference with respect to that shown by the homo-trihalide species, but they are very small in magnitude (0.05 e, at most).

On the other hand, energy decomposition methods coupled with the natural orbital for chemical valence method (EDA-NOCV) have been employed to analyze in detail the components of the interaction between X1 and X2–X3 and, above all, their dependence on the distance X1···X2. The calculations show that all the components are dependent on the nature of the halide and the asymmetry, leading to a complex pattern. In all cases, the computed charge transfers are in agreement with the CT calculated by the charge displacement method (in magnitude, as the Hirshfeld charges, or in the trend, as the charges calculated by NPA).

Our results shed new light on the experimental fact that the geometry of all the tri-halide species, in the solid state and after a normalization of the internuclear distances, can be fitted with only one equation: the effect of the charge transfer on the asymmetry is the same, or very similar, for all the combinations of halogens. However, the equation that fits the solid-state geometries can be derived from the bond-valence model,[10] and it cannot be ignored that the DFT-optimized geometry does not reproduce the trend in the structural data fitted with the BV-derived equation, but, notably, when also using the BV geometries the conclusions drawn above remain valid. The effect of the other forces in the solid state (mainly crystal packing interactions with surrounding molecules) on the X$_3^-$ geometry has been quantified by the difference in CT between the DFT and BV geometries, finding that such forces facilitate the asym-

ChemPubSoc
Europe

EurJIC
European Journal
of Inorganic Chemistry

Full Paper

metry, making it achievable with a lower charge displacement within the trihalide moiety than in the gas phase.

The results reported in this paper clearly also point out the versatility of the charge displacement method, which could find wide application in disembroiling the ongoing debate on how to define the halogen bond and other weak intermolecular interactions, and to understand their nature and origins.

Supporting Information (see footnote on the first page of this article): Additional tables and figures.

Acknowledgments

[1] a) B. Braïda, P. C. Hiberty, *Nat. Chem.* **2013**, *5*, 417–422; b) L. P. Wolters, F. M. Bickelhaupt, *ChemistryOpen* **2012**, *1*, 96–105; c) B. Braïda, P. C. Hiberty, *J. Am. Chem. Soc.* **2004**, *126*, 14890–14898.

[2] a) B. Braïda, P. C. Hiberty, *J. Am. Chem. Soc.* **2004**, *126*, 14890–14898; b) S. Riedel, T. Köchner, X. Wang, L. Andrews, *Inorg. Chem.* **2010**, *49*, 7156–7164; c) T. Vent-Schmidt, F. Brosi, J. Metzger, T. Schlöder, X. Wang, L. Andrews, C. Müller, H. Beckers, S. Riedel, *Angew. Chem. Int. Ed.* **2015**, *54*, 8279–8283; *Angew. Chem.* **2015**, *127*, 8397–8401.

[3] G. R. Desiraju, P. S. Ho, L. Kloo, A. C. Legon, R. Marquardt, P. Metrangolo, P. Politzer, G. Resnati, K. Rissanen, *Pure Appl. Chem.* **2013**, *85*, 1711–1713.

[4] L. P. Wolters, P. Schyman, M. J. Pavan, W. L. Jorgensen, F. M. Bickelhaupt, S. Kozuch, *WIREs Comput. Mol. Sci.* **2014**, *4*, 523–540.

[5] C. Wang, D. Danovich, Y. Mo, S. Shaik, *J. Chem. Theory Comput.* **2014**, *10*, 3726–3737.

[6] G. A. Landrum, N. Goldberg, R. Hoffmann, *J. Chem. Soc., Dalton Trans.* **1997**, 3605–3613.

[7] a) R. J. Hach, R. E. Rundle, *J. Am. Chem. Soc.* **1951**, *73*, 4321–4324; b) C. G. Pimentel, *J. Chem. Phys.* **1951**, *19*, 446–448.

[8] G. Manca, A. Ienco, C. Mealli, *Cryst. Growth Des.* **2012**, *12*, 1762–1771.

[9] I. D. Brown, *Chem. Rev.* **2009**, *109*, 6858–6919.

[10] M. C. Aragoni, M. Arca, F. A. Devillanova, F. Isaia, V. Lippolis, *Cryst. Growth Des.* **2012**, *12*, 2769–2779.

[11] J.-W. Zou, Y.-J. Jiang, M. Guo, G.-X. Hu, B. Zhang, H.-C. Liu, Q.-S. Yu, *Chem. Eur. J.* **2005**, *11*, 740–751.

[12] I. Alkorta, I. Rozas, J. Elguero, *J. Phys. Chem. A* **1998**, *102*, 9278–9285.

[13] A. Karpfen, *Theor. Chem. Acc.* **2003**, *110*, 1–9.

[14] L. Belpassi, I. Infante, F. Tarantelli, L. Visscher, *J. Am. Chem. Soc.* **2008**, *130*, 1048–1060.

[15] a) G. Ciancaleoni, L. Biasiolo, G. Bistoni, A. Macchioni, F. Tarantelli, D. Zuccaccia, L. Belpassi, *Chem. Eur. J.* **2015**, *21*, 2467–2473; b) G. Ciancaleoni, N. Scafuri, G. Bistoni, A. Macchioni, F. Tarantelli, D. Zuccaccia, L. Belpassi, *Inorg. Chem.* **2014**, *53*, 9907–9916; c) G. Bistoni, S. Rampino, N. Scafuri, G. Ciancaleoni, D. Zuccaccia, L. Belpassi, F. Tarantelli, *Chem. Sci.* **2016**, *7*, 1174–1184; d) K. M. Azzopardi, G. Bistoni, G. Ciancaleoni, F. Tarantelli, D. Zuccaccia, L. Belpassi, *Dalton Trans.* **2015**, *44*, 13999–14007.

[16] a) L. Rocchigiani, G. Ciancaleoni, C. Zuccaccia, A. Macchioni, *J. Am. Chem. Soc.* **2014**, *136*, 112–115; b) D. Cappelletti, E. Ronca, L. Belpassi, F. Tarantelli, F. Pirani, *Acc. Chem. Res.* **2012**, *45*, 1571–1580.

[17] a) D. Cappelletti, A. Bartocci, F. Grandinetti, S. Falcinelli, L. Belpassi, F. Tarantelli, F. Pirani, *Chem. Eur. J.* **2015**, *21*, 6234–6240; b) A. Bartocci, L. Belpassi, D. Cappelletti, S. Falcinelli, F. Grandinetti, F. Tarantelli, F. Pirani, *J. Chem. Phys.* **2015**, *142*, 184304; c) G. Ciancaleoni, C. Santi, M. Ragni, A. L. Braga, *Dalton Trans.* **2015**, *44*, 20168–20175; d) D. Cappelletti, V. Aquilanti, A. Bartocci, F. Nunzi, F. Tarantelli, L. Belpassi, F. Pirani, *J. Phys. Chem. A*, DOI: 10.1021/acs.jpca.6b00948.

[18] G. Bistoni, L. Belpassi, F. Tarantelli, *J. Chem. Theory Comput.* **2016**, *12*, 1236–1244.

[19] M. P. Mitoraj, A. Michalak, T. Ziegler, *J. Chem. Theory Comput.* **2009**, *5*, 962–975.

[20] C. Adamo, V. Barone, *J. Chem. Phys.* **1998**, *108*, 627–631.

[21] F. Weigend, R. Ahlrichs, *Phys. Chem. Chem. Phys.* **2005**, *7*, 3297–3305.

[22] a) K. A. Peterson, D. Figgen, E. Goll, H. Stoll, M. Dolg, *J. Chem. Phys.* **2003**, *119*, 11113; b) K. L. Schuchardt, B. T. Didier, T. Elsethagen, L. Sun, V. Gurumoorthi, J. Chase, J. Li, T. L. Windus, *J. Chem. Inf. Model.* **2007**, *47*, 1045–1052.

[23] J. Tomasi, B. Mennucci, R. Cammi, *Chem. Rev.* **2005**, *105*, 2999–3094.

[24] a) S. Grimme, *WIREs Comput. Mol. Sci.* **2011**, *1*, 211–228; b) E. Van Lenthe, E. J. Baerends, *J. Comput. Chem.* **2003**, *24*, 1142–1156.

[25] a) G. Te Velde, F. M. Bickelhaupt, E. J. Baerends, C. Fonseca Guerra, S. J. A. van Gisbergen, J. G. Snijders, T. Ziegler, *J. Comput. Chem.* **2001**, *22*, 931–967; b) C. Fonseca Guerra, J. G. Snijders, G. T. Velde, E. J. Baerends, *Theor. Chem. Acc.* **1998**, *99*, 391–403.

[26] a) T. Ziegler, A. Rauk, *Inorg. Chem.* **1979**, *18*, 1755–1759; b) T. Ziegler, A. Rauk, *Theor. Chim. Acta* **1977**, *46*, 1–10; c) T. Ziegler, A. Rauk, *Inorg. Chem.* **1979**, *18*, 1558–1565.

[27] a) M. Mitoraj, A. Michalak, *J. Mol. Model.* **2007**, *13*, 347–355; b) A. Michalak, M. Mitoraj, T. Ziegler, *J. Phys. Chem. A* **2008**, *112*, 1933–1939; c) M. Mitoraj, A. Michalak, *Organometallics* **2007**, *26*, 6576–6580.

[28] a) R. F. Nalewajski, J. Mrozek, A. Michalak, *Int. J. Quantum Chem.* **1997**, *61*, 589–601; b) A. Michalak, R. L. DeKock, T. Ziegler, *J. Phys. Chem. A* **2008**, *112*, 7256–7263.

[29] V. N. Staroverov, G. E. Scuseria, J. M. Tao, J. P. Perdew, *J. Chem. Phys.* **2003**, *119*, 12129–12137.

[30] A. Mancini, M. C. Aragoni, A. L. Bingham, C. Castellano, S. L. Coles (née Huth), F. Demartin, M. B. Hursthouse, F. Isaia, V. Lippolis, G. Maninchedda, A. Pintus, M. Arca, *Chem. Asian J.* **2013**, *8*, 3071–3078.

[31] F. van Bolhuis, P. B. Koster, T. Migchelsen, *Acta Crystallogr.* **1967**, *23*, 90–91.

[32] Notably, the bond length in I_2^- is 3.234 Å.

[33] H.-B. Bürgi, *Angew. Chem. Int. Ed. Engl.* **1975**, *14*, 460–473; *Angew. Chem.* **1975**, *87*, 461–475.

[34] S. V. Rosokha, C. L. Sterne, J. T. Ritzert, *Chem. Eur. J.* **2013**, *19*, 8744–8788.

[35] M. C. Aragoni, M. Arca, F. A. Devillanova, A. Gerau, F. Isaia, V. Lippolis, A. Mancini, *Bioinorg. Chem. Appl.* **2007**, art. ID 17416, 1–46 and references cited therein.

[36] A. E. Reed, R. B. Weinstock, F. Weinhold, *J. Chem. Phys.* **1985**, *83*, 735–746.

[37] When $\alpha < 1$, the fragments can be swapped, defining the halide as the atom having the larger distance from X2.